Peer-reviewed version available at Atoms 2019, 7, 61; doi:10.3390/atoms7030061

Article

Measurements of gaseous hydrogen-nitrogen laser-plasma

Christian G. Parigger [1,*]

[1] Physics and Astronomy Department, University of Tennessee, University of Tennessee Space Institute, Center for Laser Applications, 411 B.H. Goethert Pkwy, Tullahoma, TN 37388, USA; cparigge@tennessee.edu

* Correspondence: cparigge@tennessee.edu; Tel.: +1-931-841-5690

Abstract: This work communicates laser-plasma experiments in a gaseous mixture of hydrogen and nitrogen. Time-resolved spectroscopy measures the first four Balmer series hydrogen lines together with selected neutral and ionized nitrogen lines. Optical breakdown plasma is generated in a 1:1 hydrogen:nitrogen mixture at ambient temperature and 0.27-atm pressure. Time-resolved spectroscopy records emitted radiation with spatial resolution along the slit height for the H_α, H_β, H_γ, and H_δ lines. For 13 selected time delays from 0.25 μs to 3.25 μs and 0.025 μ gate-widths, micro-plasma diagnostics is evaluated. Of interest are the peak-separation and width of H_δ and width of H_γ for electron densities in the range of 0.1 to 1.0 $\times 10^{17} cm^{-3}$, and comparisons with H_β and H_α diagnostics. Integral inversions interrogate spatial distributions of the plasma expansion. Applications include laboratory and stellar astrophysics plasma diagnosis.

Keywords: atomic and molecular spectroscopy; time-resolved spectroscopy; laser plasma; laser-induced optical breakdown; stellar astrophysics spectra; white dwarf stars; hydrogen

1. Introduction

Measurement of laser-plasma gained significant attention in recent years [1,2]. Applications include determination of chemical composition of materials, but always in view of accurate descriptions from a thermodynamic point of view [3,4]. However, addition of fractionally small amounts of hydrogen [5] can be vital for analysis of plasma. Time-resolved plasma spectroscopy [6,7] requires spatial resolution for appropriate characterization of expansion phenomena and species distributions. Analysis of line-of-sight data frequently requires integral inversions [8] for detailed interpretation.

Recent hydrogen laser-plasma experiments address the first four Balmer series hydrogen lines – early in the plasma decay, neutral and ionized nitrogen lines are identified and appear first as the plasma cools. Plasma characteristics for time delays up to 0.275 μs were previously discussed for exclusively hydrogen gas at 0.75 atm and ambient temperature [9–11]. In this work, optical breakdown plasma is generated in a 1:1 hydrogen:nitrogen mixture at ambient temperature and 0.27-atm pressure. Plasma diagnosis is applied for time delays in the range of 0.25 μs to 3.25 μs [12,13]. Nitrogen contributes to the breakdown plasma seven times more electrons than hydrogen in cases of full ionization. Time-resolved spectroscopy records emitted radiation with spatial radiation along the slit height for the H_α, H_β, H_γ, and H_δ lines.

Applications of the reported work include analysis of stellar astrophysical spectra from white dwarf stars [13]. In the visible region of the electromagnetic spectrum, H_β is of primary interest in the characterization of white dwarf (WD) stars. However, comparisons of hydrogen Balmer series emission lines with recorded astrophysical WD absorption lines requires bound-free opacity corrections [14]. The temperature of the closest WD to earth, Sirius B (α CMa B), is of the order of 30 kK. Sirius B accompanies the brightest star Sirius A, as seen from earth. However, challenges in comparisons of laboratory and astrophysical plasma-spectra have been reviewed recently [15], i.e., comparisons of H_β line shapes of micro-plasma recorded with time-resolved emission spectroscopy and of H_β line

shapes in astrophysical white dwarf macro-plasma absorption spectra that are measured continuously at various observatories.

2. Materials and Methods

Laboratory laser-plasma measurements employ a pulsed, Q-switched, Nd:YAG laser device (Q-Smart 850 Quantel laser, USA) operated at a pulse-width of 6 ns and a pulse energy of 850 mJ at the wavelength of 1064 nm. Laser-induced optical breakdown is generated by focusing 150 mJ per pulse of ir fundamental radiation to achieve of the order of 1 TW/cm^2 in a cell containing a 1:1 mixture of hydrogen and nitrogen, introduced at a pressure of 0.135 atm each after establishing a nominal mercury-diffusion-pump vacuum in the cell of the order 10^{-5} mbar. A crossed Czerny–Turner spectrometer (Jobin Yvon 0.64 m triple spectrometer, France) of 0.64-nm focal length disperses the emission spectra. The pulsed radiation is focused into the cell with the beam propagating from the top and parallel to the vertical 100 μm spectrometer slit. Further details of the experimental arrangement that is similar to the ultra-pure hydrogen experiments were communicated previously [9–11].

The spectral resolution amounts to 0.1 nm for the selected 1200 g mm^{-1} holographic grating following corrections of the wavelength variation along the slit direction [12]. Of the order of 24-nm spectral coverage for the 1024 pixels along the wavelength-dimension, the 0.1-nm resolution corresponds to an instrument-prompt width of on-average 4.25 pixels. Grouping four pixels along the slit dimensions corresponds to a spatial resolution of 54.4 μm as the pixel area amounts to 13.6 μm $\times$ 13.6 μm.

3. Results

For 13 selected time delays from 0.25 μs to 3.25 μs and 0.025 μs gate-widths, micro-plasma data are captured. Of interest are the peak-separation and width of H_δ and width of H_γ for electron densities in the range of 0.1 to 1.0 $\times 10^{17}$ cm^{-3}, and comparisons with H_β and H_α diagnostics. Integral inversion interrogates the lateral spatial distribution of the recorded line-of-sight plasma expansion.

3.1. Line-of-sight measurements

A total of 52 two-dimensional data sets are recorded for the four H_α, H_β, H_γ, and H_δ Balmer series lines, including several nitrogen and ionized nitrogen lines especially for time delays in the range of 0.25 - 0.75 µs following plasma initiation. Figures 1 to 4 illustrate spectral radiance, pseudo-colored, individually scaled maps of the four hydrogen lines for time delays of 0.75, 1.5, 2.25, and 3.25 µs.

Features of Figure 1 include, (i) full-widths at half maximum increase from the H_α line to the H_γ line; (ii) the maximum decreases from H_α to H_γ; (iii) occurrence of a neutral nitrogen line near 399 nm in the H_γ map above a uv-shaded background – the broad H_γ line will show a peak separation for larger time delays; (iv) peak-separation of the H_β line, or the occurrence of a dip – this dip is not due to self-absorption – prediction of the Stark effect on the H_β line is part of the reason for E. Schrödinger [16] being awarded the Nobel Prize in Physics in 1933 [17], shared with P. Dirac.

In the images, detector dark-counts or background contributions are subtracted, sensitivity calibrations by reference to standard lamps are applied, and linear wavelength calibration is performed with penray lamps and by using calibrated spectrometer dials. The image of the spectrometer slit usually is slightly curved near the edges, consequently, wavelength calibrations are performed for each spectrum recorded along the slit. For the experiments reported here, four vertical pixels are combined to increase sensitivity requiring 256 individual wavelength calibrations for each of four spectrometer positions. The 256 recorded, wavelength calibrated Balmer series spectra are slightly shifted and interpolated for display of the data versus slit height and wavelength position. In other words, the displayed maps are corrected for wavelength variations along the slit dimension.

The spectral resolution amounts to 0.1 nm for the selected 1200 g/mmm holographic grating and with the applied corrections for the wavelength variation along the slit direction. Of the order of 24-nm spectral coverage for the 1024 pixels along the wavelength-dimension, the 0.1-nm resolution

Peer-reviewed version available at Atoms 2019, 7, 61; doi:10.3390/atoms7030061

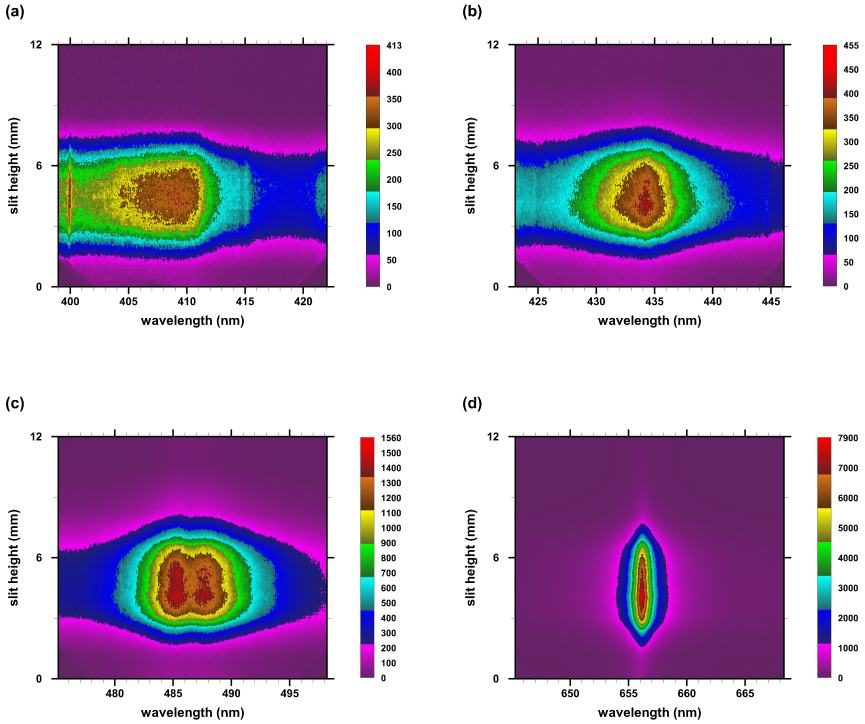

Figure 1. Recorded Balmer series hydrogen lines at 0.75-μs time delay, 0.025-μs gate. **(a)** H_δ, **(b)** H_γ, **(c)** H_β, and **(d)** H_α.

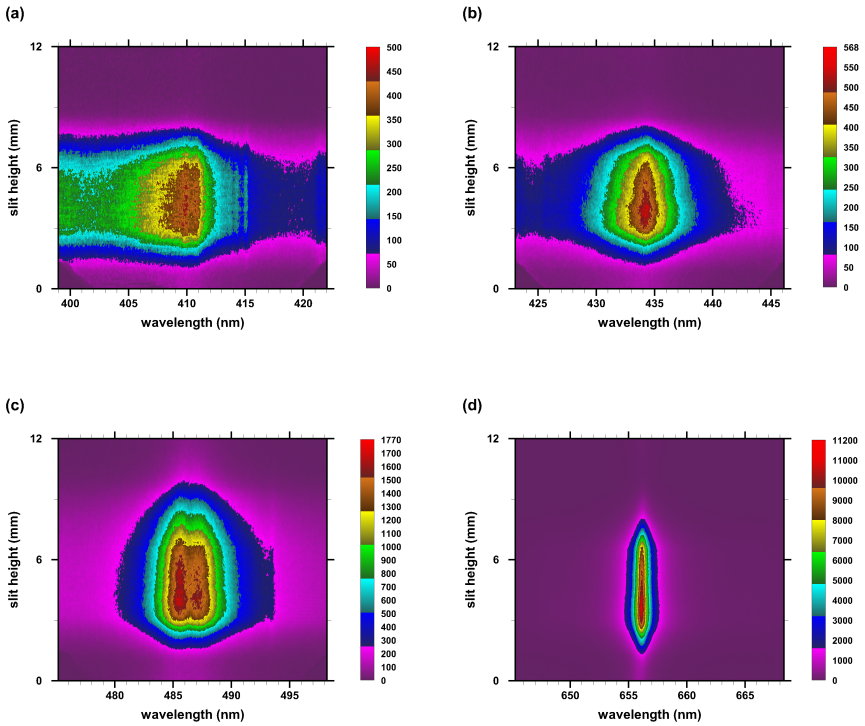

Figure 2. Recorded Balmer series hydrogen lines at 1.5-μs time delay, 0.025-μs gate. **(a)** H_δ, **(b)** H_γ, **(c)** H_β, and **(d)** H_α.

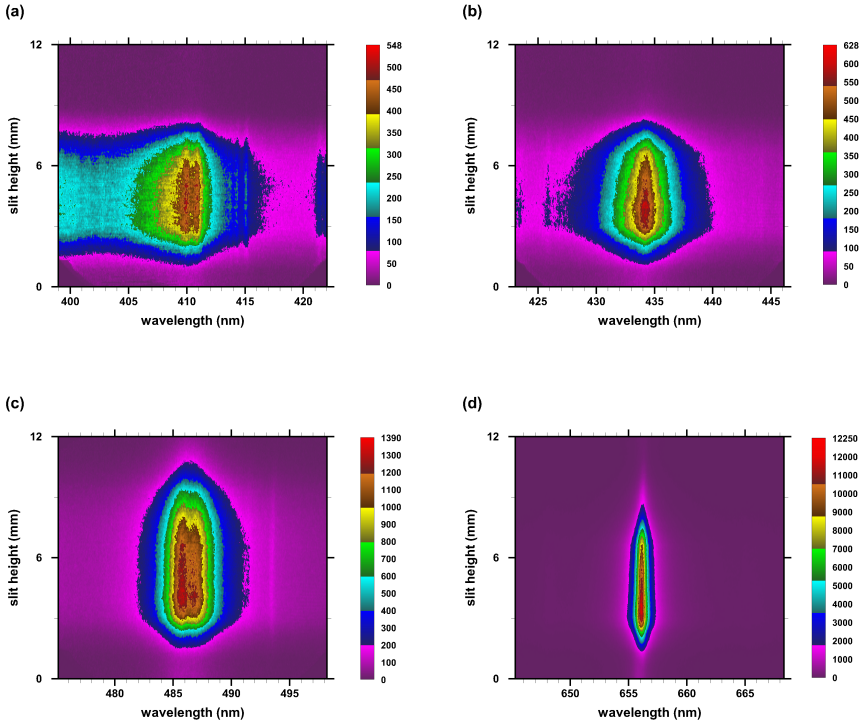

Figure 3. Recorded Balmer series hydrogen lines at 2.25-μs time delay, 0.025-μs gate. **(a)** H_δ, **(b)** H_γ, **(c)** H_β, and **(d)** H_α.

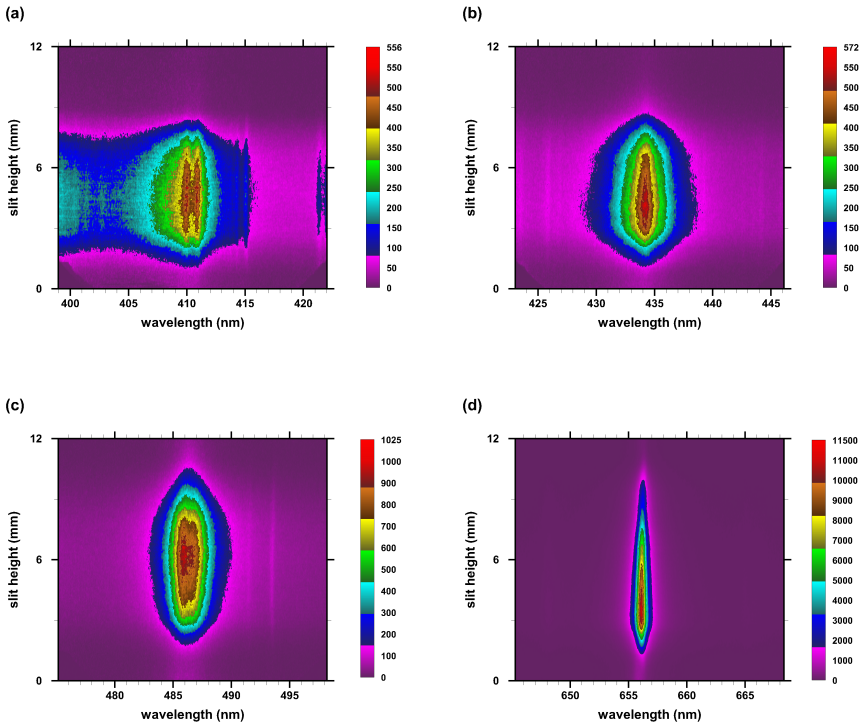

Figure 4. Recorded Balmer series hydrogen lines at 3.25-μs time delay, 0.025-μs gate. **(a)** H_δ, **(b)** H_γ, **(c)** H_β, and **(d)** H_α.

corresponds to an instrument-prompt width of on-average 4.25 pixels. Conversely, grouping four pixels along the slit dimensions corresponds to a spatial resolution of 54.4 µm as the pixel area amounts to 13.6 µm × 13.6 µm.

Analysis of the laboratory emission spectra utilizes established empirical formulae for H_α and H_β [9]. For H_α, the width, $\Delta\lambda_\alpha$, and shift, $\delta\lambda_\alpha$, are indicators for electron density,

$$\Delta\lambda_\alpha[\mathrm{nm}] = 1.3\left(\frac{N_e[\mathrm{cm}^{-3}]}{10^{17}}\right)^{0.64\pm0.03}, \quad (1)$$

$$\delta\lambda_\alpha[\mathrm{nm}] = 0.055\left(\frac{N_e[\mathrm{cm}^{-3}]}{10^{17}}\right)^{0.97\pm0.03}. \quad (2)$$

Analysis of H_β offers three indicators of electron density: Width, $\Delta\lambda_\beta$, peak separation, $\delta\lambda_{\beta-\mathrm{ps}}$, and dip shift, $\delta\lambda_{\beta-\mathrm{ds}}$,

$$\Delta\lambda_\beta[\mathrm{nm}] = 4.5\left(\frac{N_e[\mathrm{cm}^{-3}]}{10^{17}}\right)^{0.71\pm0.03}, \quad (3)$$

$$\delta\lambda_{\beta-\mathrm{ps}}[\mathrm{nm}] = 1.3\left(\frac{N_e[\mathrm{cm}^{-3}]}{10^{17}}\right)^{0.61\pm0.03}, \quad (4)$$

$$\delta\lambda_{\beta-\mathrm{ds}}[\mathrm{nm}] = 0.14\left(\frac{N_e[\mathrm{cm}^{-3}]}{10^{17}}\right)^{0.67\pm0.03}. \quad (5)$$

The H_β dip-shift allows one to measure electron density [10] up to the H_β Inglis-Teller limit [18] of $60 \times 10^{17}\mathrm{cm}^{-3}$. However, H_β is preferred in a variety of astrophysics data-reduction efforts for electron densities of the order of $10^{17}\mathrm{cm}^{-3}$.

3.2. H_δ and H_γ line profiles

The analysis of the H_δ and H_γ data rely on computer simulations [19], and in this work, on published Stark tables [20] that only show electron-density data in the range of 0.1 to 1×10^{17} cm^{-3} for a temperature of 20 kK. From the Stark tables, H_δ and H_γ line-profiles can be constructed for electron densities, N_e, of 0.1 and 1×10^{17} cm^{-3}. Subsequently, H_δ and H_γ full-width half maximum (FWHM) can be determined for plasma diagnosis, moreover, H_δ invites the use of peak separation (PS) as a diagnostic tool. The recorded data display expected Stark-effect trends [20–23].

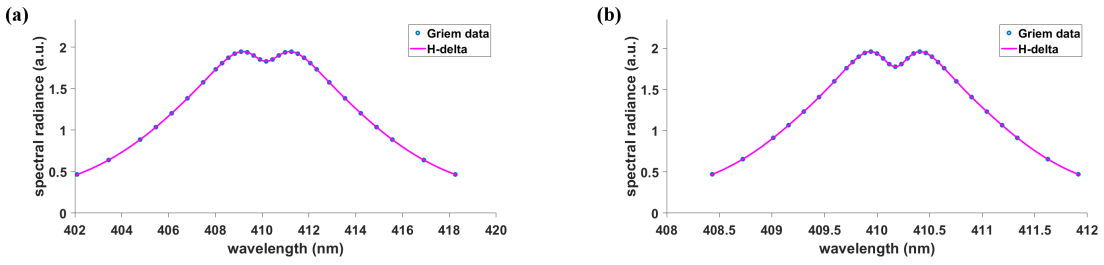

Figure 5. Computed Balmer series H_δ lines at a temperature of 20 kK. **(a)** $N_e = 1 \times 10^{17}\mathrm{cm}^{-3}$, FWHM: 10 nm, PS: 2.0 nm. **(b)** $N_e = 0.1 \times 10^{17}\mathrm{cm}^{-3}$, FWHM: 2.2 nm, PS: 0.5 nm.

From log-log fitting of H_γ and H_δ tables, see Figs. 5 and 6, in the range of 0.1 - $1 \times 10^{17}\mathrm{cm}^{-3}$, one obtains for H_δ FWHM, $\Delta\lambda_\delta$,

$$\Delta\lambda_\delta[\mathrm{nm}] = 10\left(\frac{N_e[\mathrm{cm}^{-3}]}{10^{17}}\right)^{0.67}, \quad (6)$$

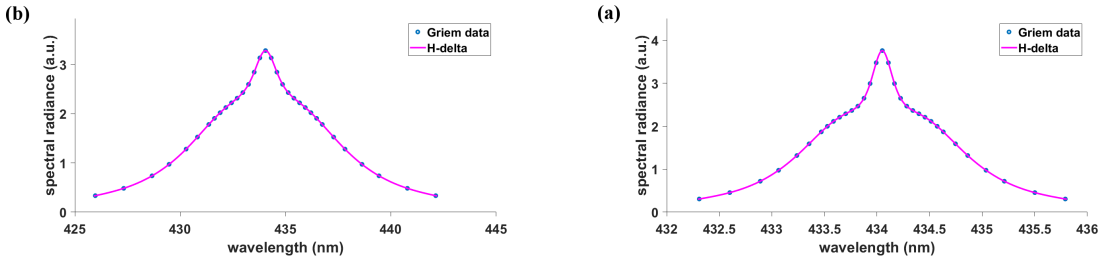

Figure 6. Computed Balmer series H_γ lines at a temperature of 20 kK. **(a)** $N_e = 1 \times 10^{17} cm^{-3}$, FWHM: 6.0 nm. **(b)** $N_e = 0.1 \times 10^{17} cm^{-3}$, FWHM: 1.15 nm.

and the H_δ peak-separation, $\Delta\lambda_{\delta-ps}$, in the range of 0.1 - 1. $\times 10^{17} cm^{-3}$ amounts to

$$\Delta\lambda_{\delta-ps}[nm] = 2.0 \left(\frac{N_e[cm^{-3}]}{10^{17}} \right)^{0.62}. \quad (7)$$

The H_δ shows peak separations just like those for the H_β line [24]. The appearance of the H_γ line is perhaps unusual in view of the H_α line, but Fig. 6 portrays the line-shape modifcations due to the Stark effect. From log-log fitting, one obtains for H_γ FWHM, $\Delta\lambda_\gamma$,

$$\Delta\lambda_\gamma[nm] = 6.0 \left(\frac{N_e[cm^{-3}]}{10^{17}} \right)^{0.72}. \quad (8)$$

3.3. Abel-inverted spectral maps

The recorded line-of-sight data are further processed using inverse Abel transform in order to examine the spatial distribution of the expanding plasma. The wavelength variation along the slit dimension is corrected for each spectral line of a single slit-height versus wavelength map. Consequently, the maps in Figures 1 to 4 are primed for analysis of integral inversion of the recorded line-of-sight data. Figures 7 and 9 illustrate the spectral radiance as function of radius and wavelength for time delays of 1.5 and 3.25 µs, respectively.

For the 1.5 µs data, the Abel-inverted, first four Balmer series lines reveal minima at the center of the plasma. These minima are representative of plasma expansion phenomena following initiation of optical breakdown. Figs. 7(a) and 7(c) reveal peak separation of the H_δ and H_β lines, respectively. The H_δ map also indicates a background shaded towards the uv, and there appear to be contributions from the H_ϵ line (at the low wavelenght side in the map). The H_δ line shows a shallower dip for higher electron density as illustrated in the range of 0.1 to 1 $\times 10^{17} cm^{-3}$ for Fig. 5. However, the H_β peak separation indicates an electron density of $1.5 \times 10^{17} cm^{-3}$.

The Abel-inverted, 3.25 µs time-delay data display reasonably smooth lineshapes for all four Balmer series lines. The H_δ peak separation can be easily demarcated, but the H_β peak separation is difficult to extract. In other words, The H_δ line provides both peak separation and FWHM diagnostics as the electron density decreases in the range of 1.0 to 0.1 $\times 10^{17} cm^{-3}$. A 1-nm peak separation of the H_δ line in Fig. 9(a) implies $N_e = 0.33 \times 10^{17} cm^{-3}$.

Both Figures 7 and 9 indicate undulations of the signal along the radial direction. Such undulations can be expected as the laser-plasma expands – in related experiments of optical breakdown in air, multiple reflections can be seen in shadowgraphs that are captured following optical breakdown in air. Similar behavior is expected to occur for the hydrogen:nitrogen mixture. Fig. 8 displays recorded air-breakdown shadowgraph to further elucidate multiple reflections that are likely causing undulations in the plasma core. The shadowgraph experiments recorded 125 images for each time delay, the selected images portray typical images.

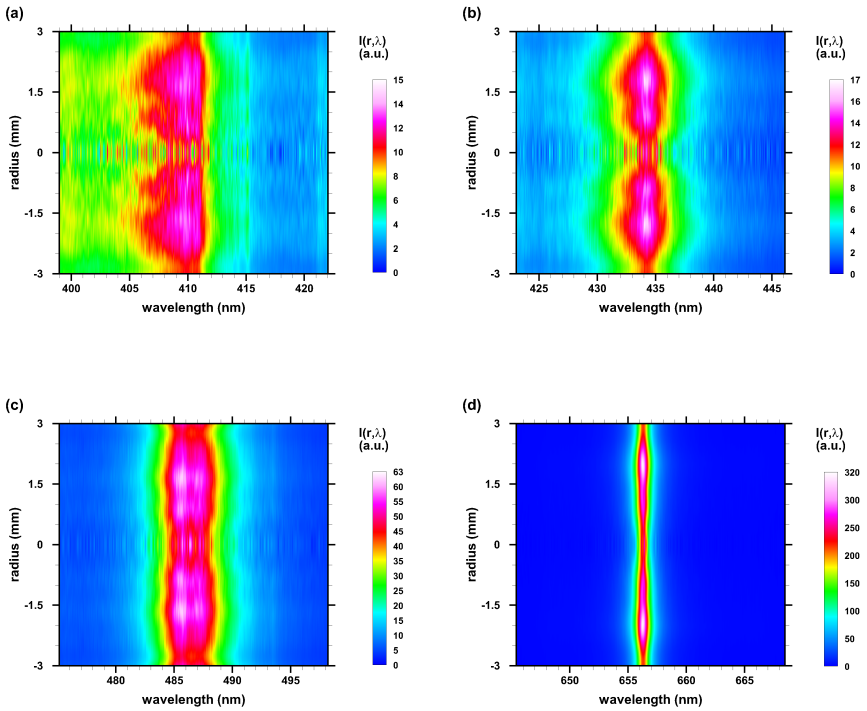

Figure 7. Abel-inverted Balmer series hydrogen lines at 1.5-µs time delay, 0.025-µs gate. **(a)** H_δ, **(b)** H_γ, **(c)** H_β, and **(d)** H_α.

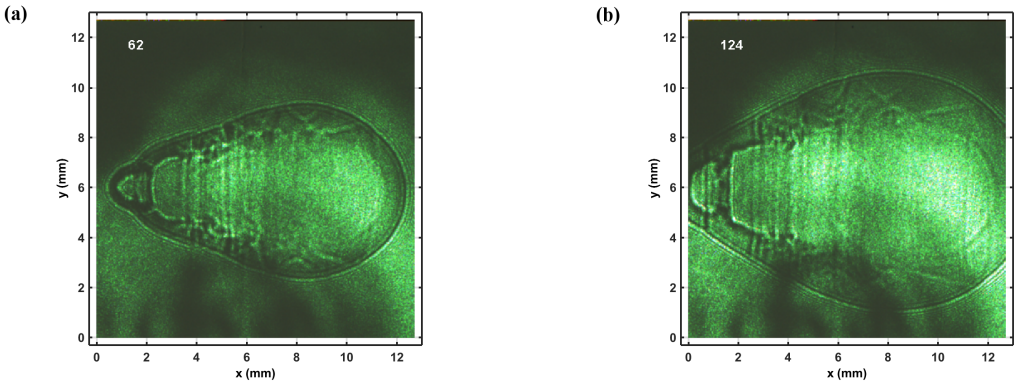

Figure 8. Shadowgraph of optical breakdown in laboratory air. The laser beam propagates from the right, images are captured using a second, imaging laser. The “bubble" on the laser side indicates absorption of laser radiation. Time delay: **(a)** 1.5 µs, image 62. **(b)** 3 µs, image 124.

3.4. Electron temperature and density

Analysis of the recorded spectra along the slit height aims to evaluate electron temperature, T_e, from Boltzmann plots. Moreover, electron density, N_e, determination relies on formulae and tables that describe Stark broadening in laser-plasma.

Figure 10 portrays typical Boltzmann plots from line-of-sight measurements at time delays of 2.25 and 3.25 µs. The method utilizes Boltzmann distributions and determination of the slope to extract the temperature from the negative of 1/slope. The intercept of the straight line is not used for evaluation of the temperature. For data points from the four Balmer series members close to the fitted line, one can infer local thermodynamic equilibrium. As the data points deviate from the fitted line, deviations

Preprints (www.preprints.org) | NOT PEER-REVIEWED | Posted: 14 June 2019 doi:10.20944/preprints201906.0134.v1

Peer-reviewed version available at Atoms 2019, 7, 61; doi:10.3390/atoms7030061

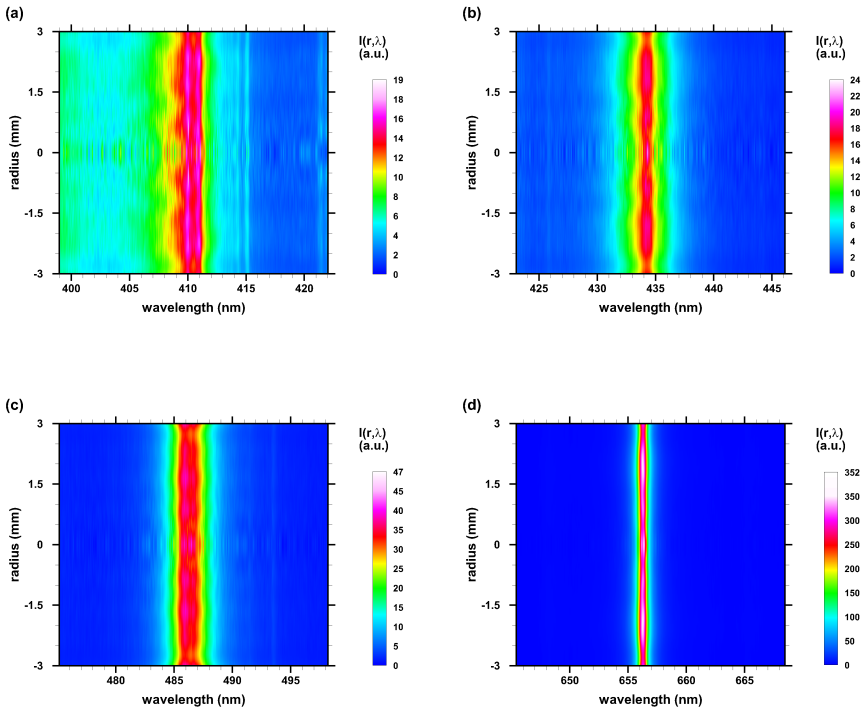

Figure 9. Abel-inverted Balmer series hydrogen lines at 2.25-μs time delay, 0.025-μs gate. **(a)** H_δ, **(b)** H_γ, **(c)** H_β, and **(d)** H_α.

from equilibrium may be concluded – self-absorbed lines would also cause deviations of data points from the straight line, and equally, ambiguities in determination of the baseline. However, expansion dynamics may lead to variations in the integrated line intensities leading to a 25% estimate for the accuracy of the inferred temperature.

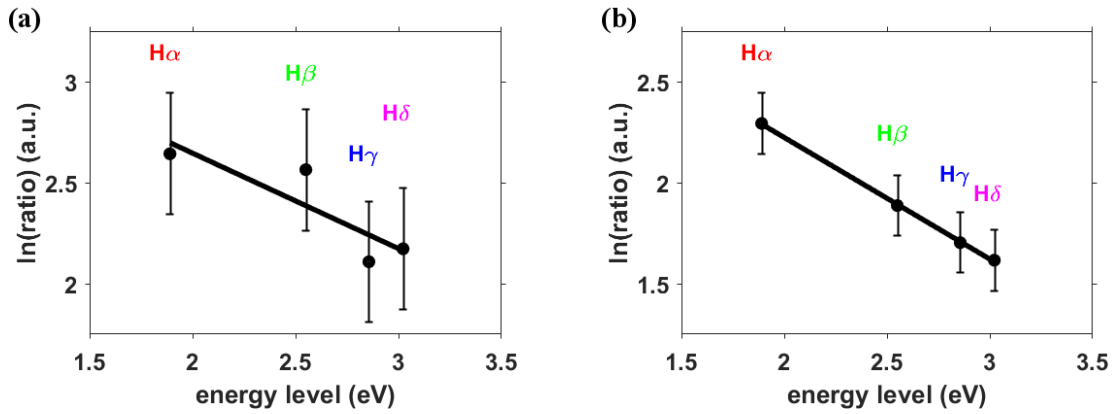

Figure 10. Boltzmann plot from line-of-sight data at 4.8-mm slit height. **(a)** T = 26.5 kK, time delay 1.5 μs (Fig. 2). **(b)** T = 19.3 kK, time delay 3.25 μs (Fig. 4).

The electron density is related to the hydrogen Balmer series FWHM to the power of the order of 1.5, however, detailed theory predictions and experimental results indicate slight deviations. Empirical equations are obtained from log-log fitting of FWHM and electron density. For red-shift of the H_α line, the dependency on electron density is almost linear. Significant new results also utilize peak-separation of the H_β line to find N_e. Stark broadening widths increase from H_α to H_γ. The use of H_β peak-separation for N_e determination in laser-plasma adds a new diagnostic tool. Investigations

of the H_δ peak separation is communicated for N_e in the rang of 0.1 to 1 $\times 10^{17} cm^{-3}$ and for the hydrogen-nitrogen laser plasma. Table 1 displays measured FWHM and peak-separations. The values are determined from the spectra at a slit height of 4.8 mm by using Matlab® software "peakfit.m" [25]. Table 2 reports the corresponding electron densities.

Table 1. First four Balmer series FWHM and H_δ and H_β peak-separations from line-of-sight data at 4.8-mm slit height.

τ [μs]	$\Delta\lambda_\delta$ [nm]	$\Delta\lambda_{\delta-ps}$ [nm]	$\Delta\lambda_\gamma$ [nm]	$\Delta\lambda_\beta$ [nm]	$\Delta\lambda_{\beta-ps}$ [nm]	$\Delta\lambda_\alpha$ [nm]
1.50	7.5 ± 1.5	1.4 ± 0.8	5.0 ± 0.2	4.2 ± 0.25	1.2 ± 0.2	1.17 ± 0.1
3.25	5.8 ± 0.3	1.1 ± 0.2	3.2 ± 0.2	2.6 ± 0.25	0.8 ± 0.15	0.78 ± 0.1

Table 2. First four Balmer series electron densities, N_e $[10^{17} cm^{-3}]$, from line-of-sight data at 4.8-mm slit height.

τ [μs]	$N_e(\delta)$	$N_e(\delta - ps)$	$N_e(\gamma)$	$N_e(\beta)$	$N_e(\beta - ps)$	$N_e(\alpha)$	average N_e
1.50	0.65	0.56	0.77	0.91	0.88	0.84	**0.77**
3.25	0.44	0.38	0.41	0.46	0.46	0.45	**0.43**

For the 3.25-μs time delay, electron densities largely agree when inferred from the widths of the four Balmer series lines and from the peak-separations of H_β and H_δ. However, there are subtle differences of N_e determined at 1.5 μs time delay. One may conclude from the appearance of the measured emission spectra and the computed Abel-inverted spectra that super- to hyper- sonic laser-plasma expansion speeds affect the establishment of local thermodynamic equilibrium. Details are investigated in the next section.

3.5. Plasma expansion dynamics

Laser-plasma generation with laser pulses of the order of 10 ns and pulse energies of 80 to 800 mJ ambient laboratory conditions causes a shock wave that expands at a rate of one to a few mm per μs, or a few km/s, for time delays of the order of 1 μs. Early in the plasma decay, expansion speeds of up to 80 km/s are usually encountered that may be described in engineering terms as well above re-entry speeds or high hypersonic speeds. Several tens of microseconds after plasma initiation, the shock wave reduces to the speed of sound.

In view of the "bubble" expanding in air and the associated isentropic expansion, one can determine electron density or temperature to elucidate the phenomena. Captured shadowgraphs can guide time-resolved spectroscopy, however, there should be an indication of the shockwave in spatially- and temporally- resolved measured spectra. One approach may utilize Radon- or Abel-inversion techniques [8] that are generally known as computed tomography methods. Or one may closely investigate the captured spectra along the slit height.

Systematic determination of the Stark widths from line-of-sight data is expected to reveal an higher electron density near the shock wave than in the plasma core. Alternatively, determination of the area of the atomic Balmer series lines should indicate higher temperature near the shock wave than in the plasma center. Moreover, for time delays of several μs – as the shockwave expanded beyond the interrogated volume – the plasma is expected to be homogeneous and indicate local thermodynamic equilibrium for electron densities in excess of 10^{16} cm^{-3}, as indicated by the necessary McWhirter criterion [3,4], but with higher temperature in the core.

Figures 11 compares electron density results for a time delay of 1.5 μs. Increases in electron density at the plasma edges are indications of the expanding shock wave. In order to estimate the

Peer-reviewed version available at Atoms 2019, 7, 61; doi:10.3390/atoms7030061

shock wave radius as function of time delay, τ, it is advantageous to utilize the Taylor-Sedov formula [26] for speherically expanding plasma,

$$R(\tau) = \left(E_p/\rho\tau^2\right)^{1/5}, \tag{9}$$

where the laser-pulse energy, E_p, for the experiments amounts to 0.15 J, and the density of the 1:1 nitrogen hydrogen mixture, ρ, equals 0.37 kg/m^3. For $\tau = 1.5$ µs, one finds for the radius $R = 4$ mm. Fig. 12 illustrates sepctroscopic snapshots of the determined temperature for $\tau = 1.5$ µs and $\tau = 2.5$ µs.

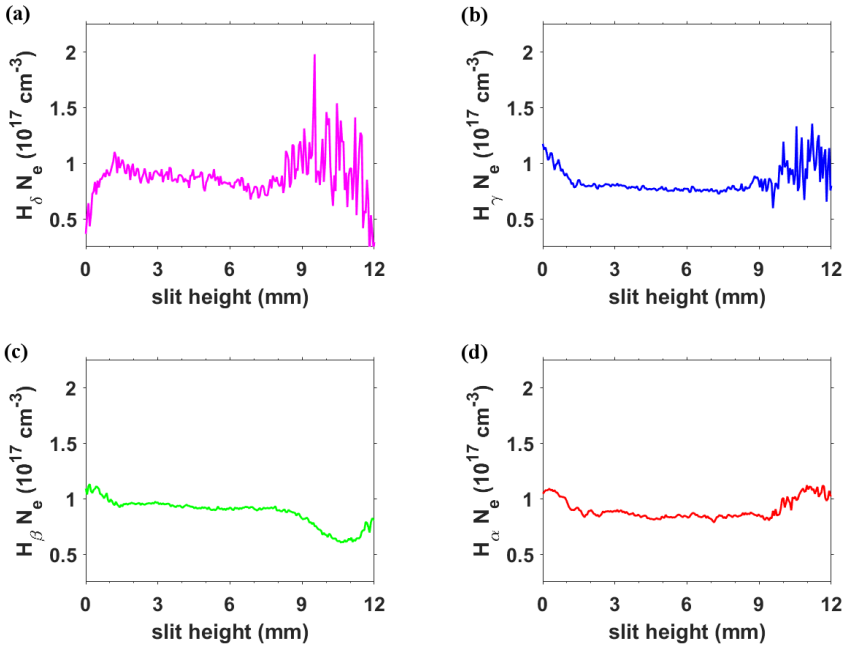

Figure 11. Electron density from line-of-sight data displayed in Fig. 2 at τ = 1.5 µs, 0.025-µs gate. **(a)** H_δ, **(b)** H_γ, **(c)** H_β, and **(d)** H_α.

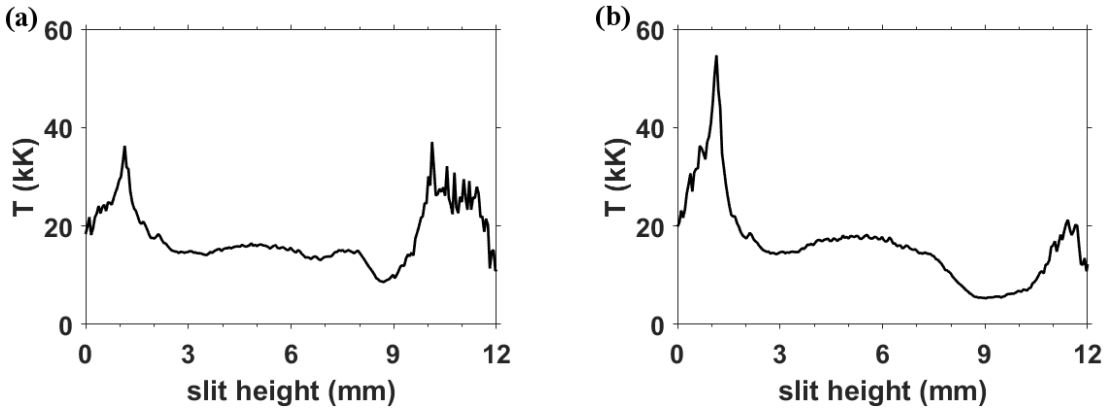

Figure 12. Electron temperature from line-of-sight data. **(a)** τ = 1.5 µs, 0.025-µs gate. Average temperature: 17.9 kK. **(b)** τ = 2.5 µs, 0.025-µs gate. Average temperature: 16.3 kK.

4. Discussion

The experimental study of H_γ and H_δ line shapes shows that results are obtained that are consistent with those from H_α and H_β, especially for time delays of the order of a few µs after initiation of laser-plasma. Shock waves tend to propagate at speeds of the order of one mm/µs for

the 0.27-atm hydrogen nitrogen mixture. Investigations of time-resolved spectra for time-delays of the order of 0.25 to 1.5 μs reveal effects from the expanding shock wave. Analysis of spectra that are recorded along the slit dimension indicate a temperature profile that is expected from computations of shock wave expansions. Abel-inverted spectra confirm the shock-wave increase of temperature and electron density, including a reduced temperature and density profile in the center of the expanding micro-plasma.

The explored H_γ and H_δ lines can provide additional diagnostics laser-plasma and for analysis of white dwarf spectra, especially in the range of 0.1 to 1 $\times 10^{17} \mathrm{cm}^{-3}$. However, when using all four lines of the Balmer series, bound-free opacity corrections would be required for comparisons of laboratory emission with white dwarf absorption spectra. Analysis of white-dwarfs and other astrophysical objects such as active galactic nuclei from only one line, i.e., H_β may be preferred as bound-free effects may not be significant across one line and for purposes of evaluation widths and asymmetries of the H_β line. Future work however should include new results from laboratory measurements that address specifically the shapes of lines for diagnosis of astrophysics phenomena.

Funding: The authors appreciate the support in part by the Center for Laser Application, a State of Tennessee funded Accomplished Center of Excellence at the University of Tennessee Space Institute.

Conflicts of Interest: The author declares no conflict of interest.

References

1. Miziolek A.W., Palleschi V., Schechter, I., Eds. 2006, *Laser Induced Breakdown Spectroscopy*; Cambridge University Press: New York, NY, USA, 2006.
2. Singh, J.P., Thakur S.N., Eds., 2019, *Laser Induced Breakdown Spectroscopy*; Elsevier Science: New York, NY, USA, 2019.; in press.
3. McWhirter, R.W.P. Spectral Intensities. *Plasma Diagnostic Techniques*; Huddlestone, R.H., Leonard, S.L., Eds.; Academic Press: New York, NY, USA, 1965; pp. 201–264.
4. Cristoforetti, G.; De Giacomo, A.; Dell'Aglio, M.; Legnaioli, S.; Tognoni, E.; Palleschi, V.; Omenetto, N. Local thermodynamic equilibrium in laser-induced breakdown spectroscopy: Beyond the McWhirter criterion. *Spectrochim. Acta Part B: At. Spectrosc.* 2010, *65*, 86–95.
5. Wiese, W.L. Line Broadening. *Plasma Diagnostic Techniques*; Huddlestone, R.H., Leonard, S.L., Eds.; Academic Press, New York, NY, USA, 1965; pp. 265–317.
6. Fujimoto T. *Plasma Spectroscopy*; Clarendon Press: Oxford, UK, 2004.
7. Kunze, H.-J. *Introduction to Plasma Spectroscopy*; Springer: New York, NY, USA, 2009; ISBN 978-3-642-02232-6.
8. Pretzler, G.; Jäger, H.; Neger, T.; Philipp, H.; Woisetschläger, J. Comparison of Different Methods of Abel Inversion Using Computer Simulated and Experimental Side-On Data. *Z. Naturforsch.* **1992**, *47a*, 955-–970.
9. Parigger, C.G.; Drake, K.A.; Helstern, C.M.; Gautam, G. Laboratory Hydrogen-Beta Emission Spectroscopy for Analysis of Astrophysical White Dwarf Spectra. *Atoms* **2018**, *6*, 6030036.
10. Parigger, C.G.; Helstern, C.M.; Gautam, G.; Drake, K.A. Atomic and molecular line shapes in laboratory and selected astrophysical plasma. *J. Phys.: Conf. Ser.*, **2019**, in press.
11. Parigger, C.G., Helstern, C.M., Gautam, G. Laser-Plasma and Self-Absorption Measurements with Applications to Analysis of Atomic and Molecular Stellar Astrophysics Spectra. Preprints 2019, 2019050364, DOI: 10.20944/preprints201905.0364.v1 .
12. Parigger, C.G.; Woods, A.C.; Witte, M.J.; Swafford, L.D.; Surmick, D.M. Measurement and Analysis of Atomic Hydrogen and Diatomic Molecular AlO, C_2, CN, and TiO Spectra Following Laser-induced Optical Breakdown. *J. Vis. Exp.* **2014**, *84*, e51250.
13. Parigger, C.G. Laser-plasma and stellar astrophysics spectroscopy. *Contrib. Astron. Obs. S.* **2019**, submitted.
14. Tremblay, P.-E.; Bergeron, P. Spectroscopic Analysis of DA White dwarfs: Stark broadening of hydrogen lines including nonideal effects. *Astrophys. J.* **2009**, *696*, 1755–1770.
15. Halenka, J.; Olchawa, W.; Madej, J.; Grabowski, B. Pressure shift and gravitational redshift of Balmer lines in white dwarfs: Rediscussion. *Astrophys. J.* **2015**, *808*, 131—140.
16. Schrödinger, E. Quantisierung als Eigenwertproblem. *Ann. Phys.* **1926**, *385*, 437-–490.

17. The Nobel Prize in Physics 1933. Available online: https://www.nobelprize.org/prizes/physics/1933/summary/ (accessed on May 24 2019).
18. Inglis, D.R.; Teller, E. Ionic depression of series limits in one-electron spectra. *Astrophys. J.* **1939**, *90*, 439–448.
19. Gigosos, M.A.; González, M.Á.; Cardeñoso, V. Computer simulated Balmer-alpha, -beta and -gamma Stark line profiles for non-equilibrium plasmas diagnostics. *Spectrochim. Acta B At. Spectrosc.* **2003**, *58*, 1489-–1504.
20. Griem, H.R. *Spectral Line Boradening by Plasmas*; Academic Press: Cambridge, MA, USA, 1974.
21. Holtsmark, J. Über die Verbreiterung von Spectrallinien. *Ann. Phys.* **1919**, *58*, 577-–630.
22. Greene, Jr., R.E. 1961, *The Shift and Shape of Spectral Lines*; Pergamon Press: Oxford, UK, 1961; Chapter 4, pp. 118–193.
23. Oks, E. 2017, *Diagnostics of Laboratory and Astrophysical Plasmas Using Spectral Lineshapes of One-, Two-, and Three-Electron Systems*; World Scientific: Singapore, 2017; pp. 1–47, ISBN 9789814699075.
24. Ivković, M.; Konjević, N.; Pavlović, Z. Hydrogen Balmer beta: The separation between line peaks for plasma electron density diagnostics and self-absorption test. *J. Quant. Spectrosc. Radiat. Trans.* **2015**, *154*, 1-–8.
25. O'Haver T.C. Command-line peak fitter for time-series signals. Version 9.0, January 2018; Mathworks File Exchange; Available online: https://www.mathworks.com/matlabcentral/fileexchange/23611-peakfit-m (accessed June 4 2019).
26. Beatrice Campanella, B.; Stefano Legnaioli, S.; Stefano Pagnotta, S.; Francesco Poggialini, F.; Palleschi, V. Shock Waves in Laser-Induced Plasmas. *Atoms* **2019**, *7*, 7020057.